Heliyon 10 (2024) e38682

Contents lists available at ScienceDirect

Heliyon

journal homepage: www.cell.com/heliyon

Research article

Synthetic and natural antibacterial carbon adsorbents for clinical nuclear waste management

Rosidah Sunaiwi [a], Ruchi Gaur [b], Mohammad Khairul Azhar Abdul Razab [a,**], Fara Hana Hadzuan [a], Norazlina Mat Nawi [c], Mohd Zahri Abdul Aziz [d], An'amt Mohamed Noor [e], Nur Atiqah Syahirah Shari [a], Zulhisyam Abdul Kari [f], Ajay Guru [g], Parashuram Kallem [h,*]

[a] *Medical Radiation Programme, School of Health Sciences, Universiti Sains Malaysia, Health Campus, 16150, Kubang Kerian, Kelantan, Malaysia*
[b] *Solid State and Structural Chemistry Unit, Indian Institute of Science, Bangalore, 560012, India*
[c] *Department of Nuclear Medicine, Radiotherapy & Oncology, School of Medical Sciences, Universiti Sains Malaysia, Health Campus, 16150, Kubang Kerian, Kelantan, Malaysia*
[d] *Department of Biomedical Imaging, Advanced Medical and Dental Institute, Universiti Sains Malaysia, Bertam, 13200, Kepala Batas, Penang, Malaysia*
[e] *Advanced Materials Research Cluster, Faculty of Bioengineering and Technology, Universiti Malaysia Kelantan, Jeli Campus, 17600, Jeli, Kelantan, Malaysia*
[f] *Department of Agricultural Sciences, Faculty of Agro-Based Industry, Universiti Malaysia Kelantan, Jeli Campus, 17600, Jeli, Kelantan, Malaysia*
[g] *Department of Cariology, Saveetha Dental College and Hospitals, Saveetha Institute of Medical and Technical Sciences, Saveetha University, Chennai, India*
[h] *Department of Environmental and Public Health, College of Health Sciences, Abu Dhabi University, Abu Dhabi, P.O. Box 59911, United Arab Emirates*

ARTICLE INFO

Keywords:
Nuclear medicine
Radioactivity
Adsorption
Morphological changes
Structural analysis

ABSTRACT

Patients undergoing high-dose radioiodine ablation (RAI) therapy in Nuclear Medicine Department need to be isolated in a special designed ward for a few days. Large amount of clinical radioactive wastewater from patient body is produced during high-activity RAI therapy. The radioactive wastewater needs to store in a delay tank until the radioactivity decayed below acceptable limit before being discharged and indirectly limit the patient admission and treatment. This study is to propose an alternative antibacterial adsorbent for I-131 extraction from clinical radioactive wastewater at the nuclear medicine department using graphene oxide silver (GOAg) and bamboo activated carbon (BAC). The synthesised adsorbents and their sediments (filtered sample) were analysed using field emission scanning electron microscopy (FESEM) for morphological analysis and analysed using X-ray photoelectron spectroscopy (XPS), Fourier transform infrared (FTIR) and X-ray diffraction (XRD). XPS spectra for C 1s adsorbents show intensity peaks at 284.45 eV (C=C) and 285.3 eV (C–C) for GOAg and its sediments, and 284.35 eV (C–C), 287.00 eV (C=O), and 290.07 eV (π–π^* transitions) for BAC and its sediments. FTIR spectra reveal various functional groups of adsorbents: C=C (1637.50772 cm^{-1}), C=O (1340.48041 cm^{-1}), and C–O–C (1031.88060 cm^{-1}) for GOAg and its sediments, and C=C (1635.57897 cm^{-1}), C–C (1257.54421 cm^{-1}), and C–O (1188.10925 cm^{-1}) for BAC and its sediments. XRD patterns exhibit peaks at $2\theta = 27.82°$, 29.39°, 32.24°, and 46.22°, which can be attributed to the (002) diffraction

* Corresponding author.
** Corresponding author.
E-mail addresses: khairul.azhar@usm.my (M.K. Azhar Abdul Razab), parashuram.kallem@adu.ac.ae (P. Kallem).

https://doi.org/10.1016/j.heliyon.2024.e38682
Received 8 June 2024; Received in revised form 26 September 2024; Accepted 27 September 2024
Available online 28 September 2024

plane, (220) crystallographic plane, (111) plane of Ag_2O, and (200) crystallographic plane, respectively, for GOAg and its sediments. Meanwhile, the peaks at $2\theta = 26.56^\circ$ and 42.41°, which correspond to (002) and (100) planes, respectively, for BAC and its sediments. The d-spacing and the crystallinity index of each adsorbent were also determined. The estimation of the remaining β^- particles during the adsorption of I-131 was carried out using PHITS. The finding of this study is beneficial for alternative radionuclide extractions technique from clinical radioactive wastewater in nuclear medicine.

1. Introduction

Nuclear medicine involved both diagnostic and therapeutic services for cancer patients through the aid of radiopharmaceuticals that administered into patient's body either orally or intravenously [1]. Radioiodine ablation therapy (RAI) is one of the common clinical treatments that widely practiced in treating thyroid cancer using I-131 radionuclide due to its non-invasive techniques and high successful rate. Patients undergoing high-dose RAI therapy need to be isolated in a specially designed ward at the nuclear medicine department [1]. The radioactive waste from the patient's body (urine and faeces) will go through a sewage system with a specially designed delay tank and will be stored to reduce the activity of clinical radioactive wastewater at a certain level, until the radioactivity decayed below the legally established acceptable limit (<1.2 μCi/L) before being discharged into the public sewer [2,3]. This is known as the delay and decay method. This method indirectly limits the number of patient admissions due to limited volume size and periodical clearance. This conditions longer the patient appointment queue and might be affected the emergency cases especially for small nuclear medicine facilities. Alternatively, this situation can be solved using concentrate and contained method, by applying antibacterial adsorbents to extract I-131 radionuclide from clinical radioactive wastewater. Previous study used Graphene Oxide to adsorb the radioactive materials in clinical radioactive wastewater, but usually focus on its absorbability and not concern about antibacterial aspects and molecular structural changes [4–6]. In this study, we conduct a series of experiments using Graphene Silver Oxide (GOAg) and bamboo activated carbon (BAC) as prominent synthetic and natural antibacterial adsorbents for I-131 radionuclide extraction. This study aims to obtain the information on the composition and morphological changes of GOAg and BAC after the adsorption of radioactive clinical wastewater at molecular level of binding energies and functional groups interactions.

Bamboo activated carbon has unique properties, such as highly porous carbonaceous material, with a high internal surface area and various functional groups. These properties result in BAC with high adsorption affinity and a faster adsorption rate for heavy metal ions [7]. Furthermore, BAC has natural antibacterial properties, which are in lignin, and these properties are important for wastewater/contaminated area cleaning [8]. Graphene oxide (GO) has various unique properties, such as physical stability, chemical stability, high specific surface area, electron mobility, and heat transfer [9]. Graphene oxide contains numerous oxygen functional groups that constitute a significant number of binding sites for Ag^+. Positively charged Ag^+ in an aqueous solution can be easily captured by negatively charged GO due to electrostatic interaction, which further promotes the antibacterial activity of GOAg [10]. The synthesis of GOAg hybrid material as a synthetic adsorbent can potentially contribute to the health sector, particularly in improving antibacterial performance and radionuclide removal. Our findings highlighted the potential innovation of radionuclide extractions based on synthetic and natural adsorbent for nuclear wastewater management in nuclear medicine.

2. Materials and methods

The experiment was carried out at the Nuclear Medicine, Radiotherapy, & Oncology Department, Hospital Universiti Sains Malaysia (HUSM) and Medical Radiation Laboratory, School of Health Sciences, Universiti Sains Malaysia.

2.1. Synthesis of graphene oxide silver

Graphene oxide was prepared using simplified Hummers' method [11]. Briefly, 3 g of graphite powder was mixed with 320 mL of sulphuric acid solution and 80 mL of phosphoric acid solution (4:1 ratio), followed by slow addition of 18 g of potassium permanganate powder. The mixture was stirred for three days using a magnetic stirrer before being poured onto 500 mL of ice cubes along with 27 mL of hydrogen peroxide (H_2O_2) solution. Then, the mixture was centrifuged at 10,000 rpm, washed three times with hydrochloric acid (HCl), followed by washing with distilled water until pH 5 was achieved. After that, 20 mM of silver nitrate ($AgNO_3$) solution was prepared by the simple dilution method, where 50 mL of distilled water was added to 0.2 g of $AgNO_3$ and stirred gently using a glass rod. Next, the synthesis of GOAg was carried out. Briefly, a few drops of ammonia (20 wt%) were added slowly into 20 mM of $AgNO_3$ solution and stirred vigorously until a clear solution was observed. Using five beakers with 3 mL of silver-ammonia solution, each beaker was mixed with 1 mL of synthesised aqueous GO earlier (3:1 vol ratio) and then homogenised for 10 min at 10,000 rpm to ensure the homogeneity of each mixture. The reaction mixture was microwave-irradiated for 30 s and then washed with distilled water (centrifuged at 9500 RCF for 15 min) until a pH of 7.46 was reached.

2.2. Synthesis of bamboo activated carbon

The BAC was prepared by the chemical activation method. First, 5 g of *Bambusa vulgaris* powder dried earlier was impregnated

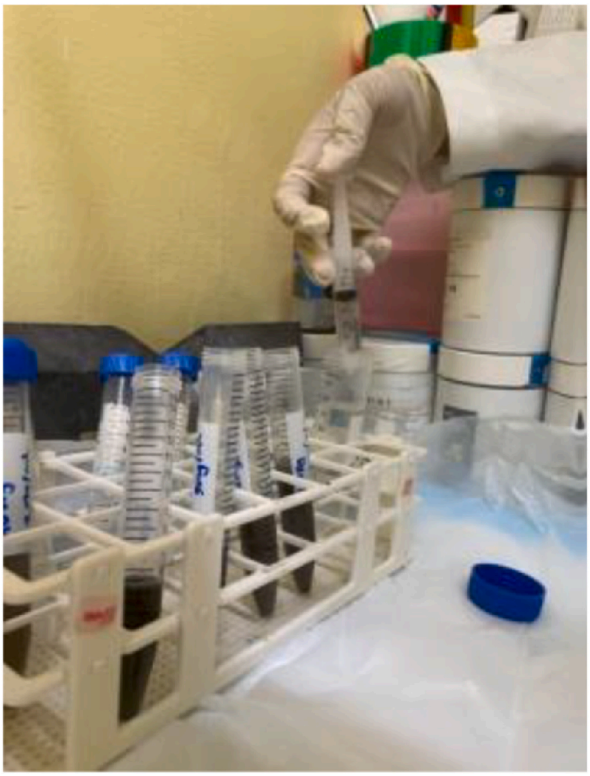

Fig. 1. Preparation of 1.0, 2.0, 3.0, 4.0 and 5.0 mg/mL concentrations of adsorbents using syringe.

Table 1
Ratio of concentration of GOAg.

Concentration of GOAg (mg/mL)	Volume of GOAg (mL)	Volume of Saline (mL)	Volume of GOAg after Dilution (mg/mL)
1.0	1.0	3.30	4.30
3.0	1.0	1.10	2.10
5.0	1.0	0.66	1.66

Table 2
Ratio of concentration of BAC.

Concentration of BAC (mg/mL)	Volume of BAC (mL)	Volume of Saline (mL)	Volume of BAC after Dilution (mg/mL)
1.0	2.0	2.50	4.50
3.0	2.0	0.83	2.83
5.0	2.0	0.50	2.50

again overnight with 5 g of potassium hydroxide (KOH) pellets and diluted by the simple dilution method. Then, the sample was carbonised in a furnace for 2 h at a carbonisation temperature of 500 °C and cooled for another 2 h. This technique is to prevent unintended reaction due to rapid cooling that leads to damage physical properties of the activated carbon [12]. The sample was washed with HCl and distilled water and then centrifuged at 10,000 rpm for 10 min until pH 6–7 was achieved to ensure that the sample was free from the base medium, followed by drying in a hot air oven for 12 h at 100 °C.

2.3. Adsorbent concentration determination and preparation

A plain filter paper was weighed using an electronic beam balance before 1 mL of absorbent was added to the filter paper and weighed. The initial concentration of 3.3 mg/mL of GOAg and 1.25 mg/mL of BAC was determined using the following equation (1) [1, 13]:

$$\text{Weight of 1 mL adsorbent} = (\text{Weight}_{\text{Adsorbent}+\text{filter paper}}) - \text{Weight}_{\text{Filter paper}}$$

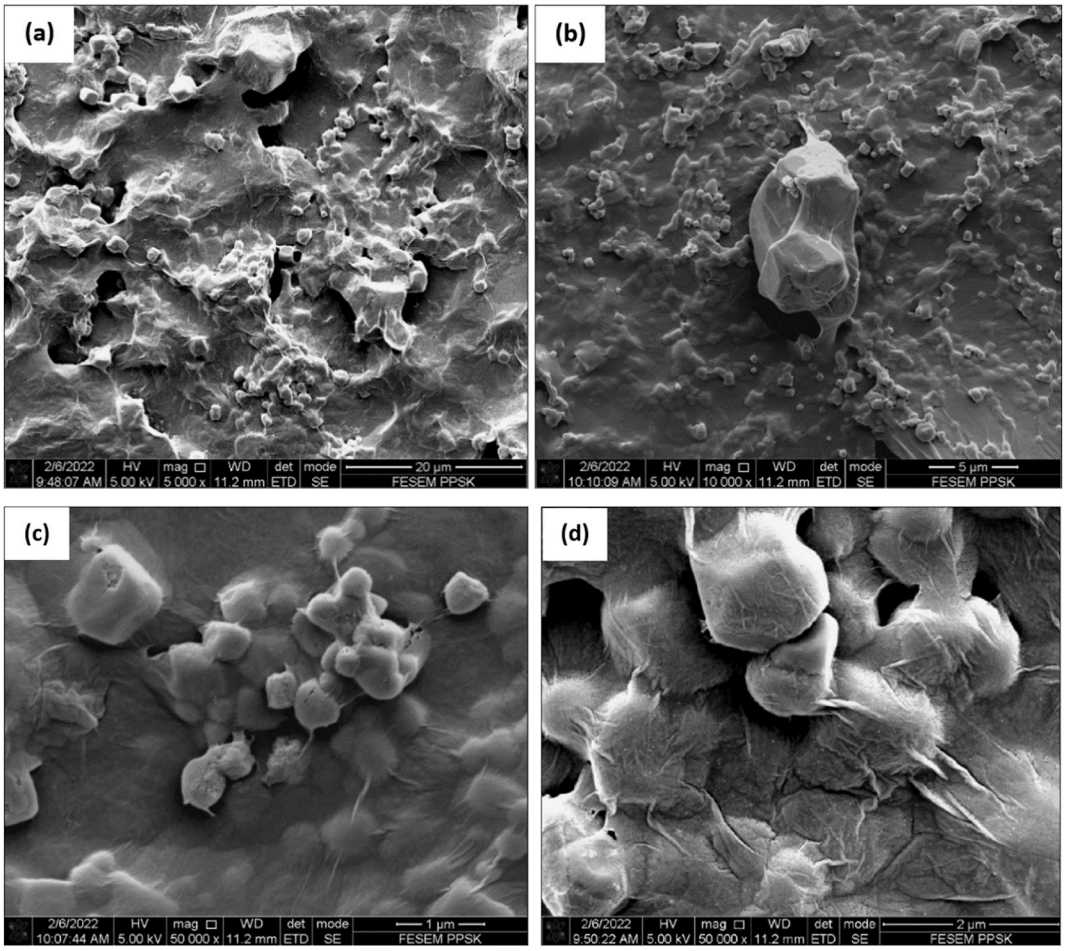

Fig. 2. FESEM images of (a) 3.3 mg/mL GOAg morphology; (b) Coated I-131:GOAg sediment; (c) Agglomerated coated sediment with GOAg and (d) Close-up coated sediments morphology interfaces attraction with stacking agglomerated structures.

$$\text{Adsorbent concentration } \left(\frac{\text{mg}}{\text{mL}}\right) = \frac{\text{Weight Adsorbent}}{\text{1 mL Adsorbent}} \quad \text{(Eq. 1)}$$

Various concentrations of adsorbents were prepared by diluting adsorbents with saline, as shown in Fig. 1. Tables 1 and 2 details the formulation of the adsorbents used, where the mixtures were calculated using Eq. (2) [5,6]:

$$M_1V_1 = M_2V_2 \quad \text{(Eq. 2)}$$

Where M_1 is the initial concentration of adsorbent (mg/mL), V_1 is the initial volume of adsorbent (mL), M_2 is the concentration of adsorbent after dilution (mg/mL), and V_2 is the volume of adsorbent after dilution (mL).

2.4. Radioactive clinical wastewater adsorption

Five bags of radioactive clinical wastewater samples with 10 mL each were obtained from a delay tank at the Nuclear Medicine, Radiotherapy, & Oncology Department, HUSM on the first day of RAI therapy. All samples were stored in a lead container before being transported to the hot laboratory. Two samples were mixed with 3.0 mg/mL of GOAg and BAC, respectively, in the hot laboratory behind the L-block radiation shield. All the samples were left for 30 min in the lead container to allow initial reactions prior to filtering. Then, each mixture was filtered using a membrane filter to obtain absorption sediment. During this experiment, the background exposure rate (mSv/h) of the delay tank room and laboratory was measured using a Geiger-Muller survey meter and an electronic pocket dosimeter for radiation safety purposes.

2.5. Morphology and characterisation

In this analysis, 3.3 mg/mL of GOAg, 1.25 mg/mL of BAC, I-131:GOAg, and I-131:BAC sediments were dropped on indium tin oxide

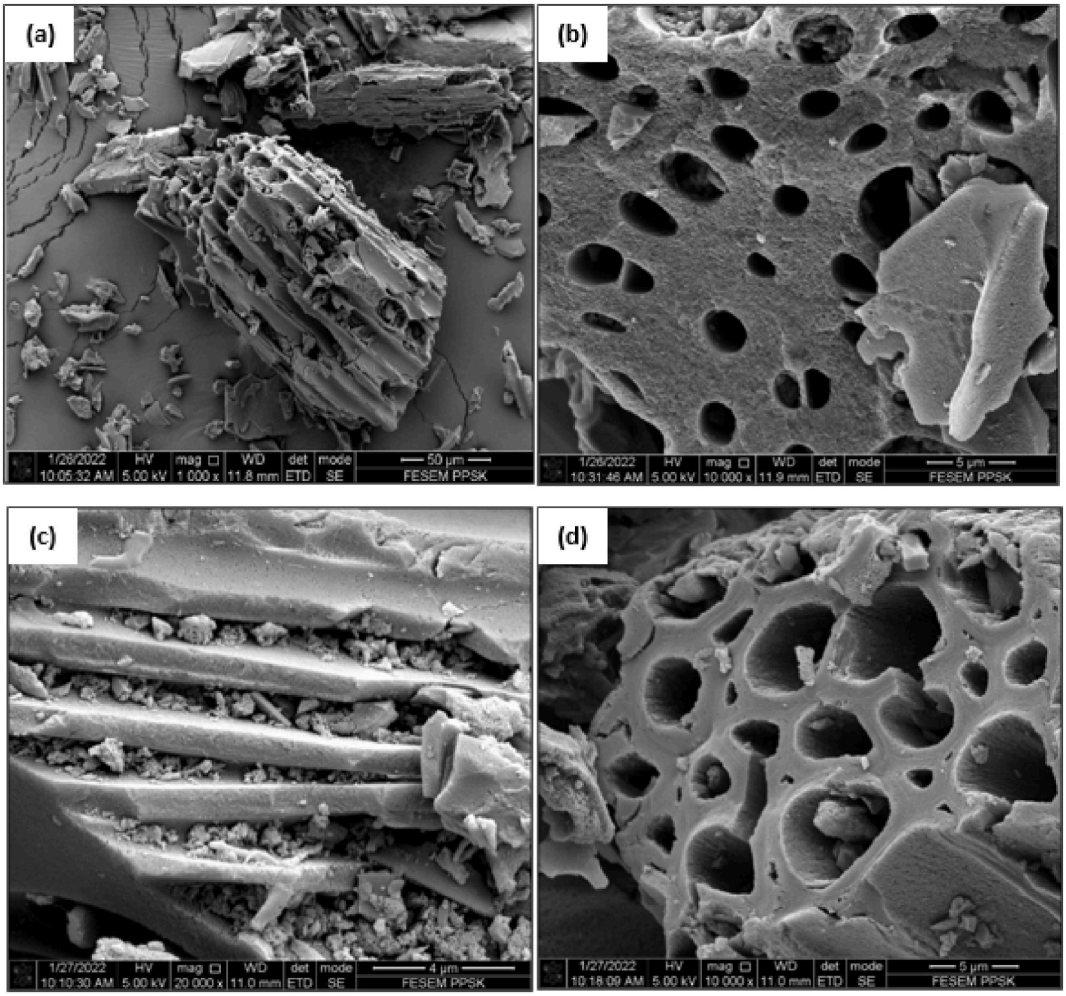

Fig. 3. FESEM images of (a) Cracks and contaminants of BAC structures on the coated substrate (b) 1.25 mg/mL BAC with small pores (c) Stacking and crack BAC layers with trapped sediments (d) I-131:BAC with large pores and sediment at 10000x magnifications.

glass substrate and left for a few days. All samples were characterised using field emission scanning electron microscopy (FESEM) to determine the morphological changes after adsorption at the SEM Laboratory, School of Health Sciences, Universiti Sains Malaysia. Each sample was coated with gold using a Leica EM-SCD005 tabletop sputter coater for 60 s at 25 mA prior to scanning with FESEM.

These samples were also analysed using Fourier transform infrared (FTIR), X-ray photoelectron spectroscopy (XPS), and X-ray diffraction (XRD) to identify the presence and appearance of chemical bonds for investigating the binding energy at the atomic level and analysing the crystallinity of pure adsorbents and sediments after adsorption of I-131 clinical wastewater.

2.6. PHITS simulation

PHITS simulation was performed to estimate the remaining beta particles during the adsorption of I-131. Three samples of radioactive clinical wastewater were mixed with GOAg and BAC at different concentrations (1.0, 3.0, and 5.0 mg/mL) and filtered using a membrane filter. The radioactivity of the residues from the filter paper and sediments after filtration was obtained using a dose calibrator over a function of time (A_0 of ^{131}I and its radioactive decay series [$A_0/4$ (day 4), $A_0/2$ (day 8), $A_0 3/4$ (day 12), and total decay (day 16)]). The estimation of the remaining beta particles during the adsorption of I-131 was performed using PHITS simulation based on Eq. (3) [1,5,6].

$$A = A_0.e^{-\lambda t} \quad \text{(Eq. 3)}$$

A = Radionuclide activity.
A_0 = Initial radionuclide activity.
λ = Decay constant
t = Decay time.

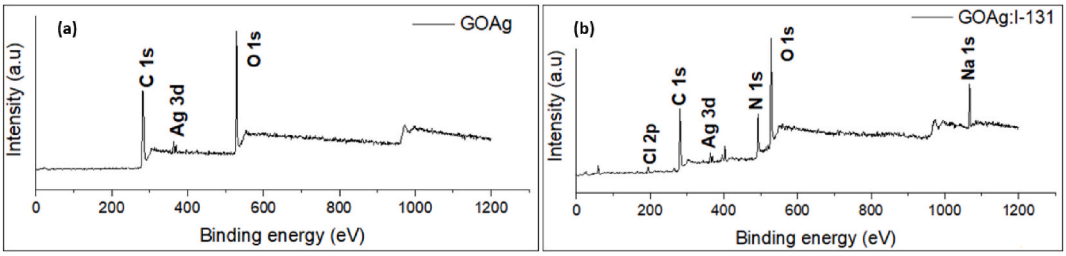

Fig. 4. Survey XPS spectra of (a) GOAg shows the normal peaks for common elements existed with 3d Ag element; (b) GOAg:I-131 shows molecular interactions occurred between GOAg, I-131 and some foreign elements in the radionuclide waste water, where three new photoelectron peaks has been detected.

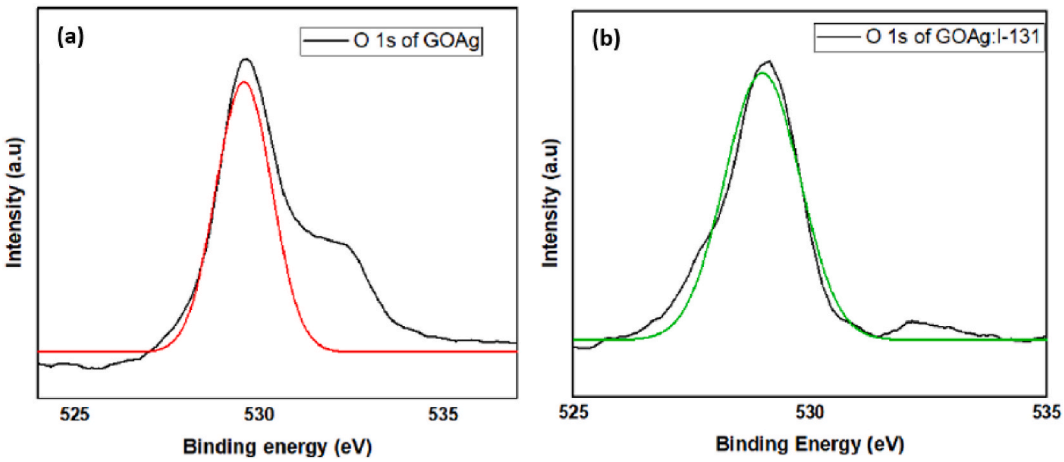

Fig. 5. O 1s core-level spectra of (a) GOAg and (b) GOAg:I-131 is almost same at 529.15 eV indicates no electron sharing between oxygen atoms and atoms in I-131 wastewater during adsorption.

The factors of adsorbent concentration and radionuclide combination were selected to investigate and validate the process parameters affecting the adsorption capability of the prepared adsorbent materials. Two independent variables involving three concentrations of adsorbents and their initial radioactivity of clinical wastewater (B_q) were investigated.

3. Results and discussion

3.1. Surface morphology of adsorbents and sediments

Fig. 2 (a) shows many uneven spots of silver (Ag) spherical nanoparticles that are randomly anchored on GO. Furthermore, Ag nanoparticles are not only evenly distributed on the surface of GO nanosheets but also inside the network [14]. This morphology was clearly demonstrated in Fig. 2 (c) with enhance magnification. This result is in line with XRD analysis, indicating the face-centred crystal (FCC) pattern of Ag and suggesting that Ag is intercalated on the surface of GO nanosheets. Fig. 2 (b) exhibits the surface morphological changes of GOAg after adsorption of I-131 wastewater. The surface morphology of the GOAg structure is depicted as the image's background layer, coating the radionuclide and forming an agglomerated structure in as shown in Fig. 2 (b) and 2 (d). The agglomerated structure suggests that I-131 was strongly trapped together with other elements in the clinical wastewater sample. This agglomerated structure is attracted by GOAg, implying that there may be an interaction between I-131 and the GOAg surface through surface complexation, as there are abundant functional groups on the GOAg surface, such as hydroxyl, carboxyl, and epoxy groups.

Meanwhile, the well-developed porous structure of various shapes and sizes was clearly visible on the synthesised BAC surface, which might be macropores, mesopores, or micropores, as shown in Fig. 3 (a) and 3 (b) distinctly demonstrates an incomplete porous surface containing broken scratches of the porous surface's edge, which may be due to trituration [15]. Bamboo activated carbon has relatively large pores suitable for large molecule adsorption as shown in Figures (b) and (d) [16]. Furthermore, well-developed pores resulted in a large surface area of the synthesised BAC [17]. Comparatively, the longitudinal section of the synthesised BAC in Fig. 3(b) was loaded with contaminants, which are I-131 and other elements in the wastewater sample resulting from the adsorption process. This proves the success of the activation process as the synthesised BAC efficiently trapped the I-131 wastewater [18]. Moreover, it can be observed in Fig. 3(c) that there were cracks on some of the porous structures on the transverse section of BAC, which may be due to the clogging of I-131 wastewater during adsorption.

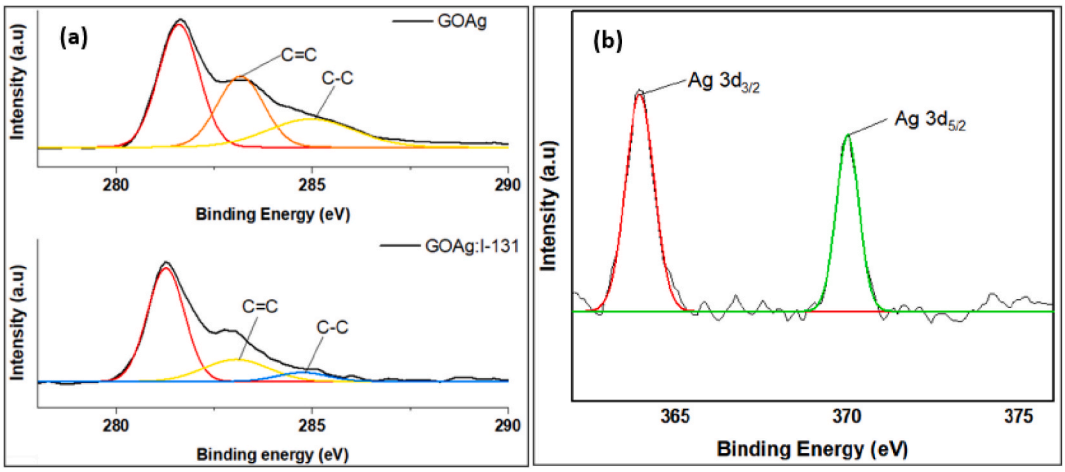

Fig. 6. (a) C 1s core-level spectra of GOAg and GOAg:I-131 before and after adsorption (b) Ag 3d core-level spectra existed on GOAg at 364.15 eV and 370.05 eV.

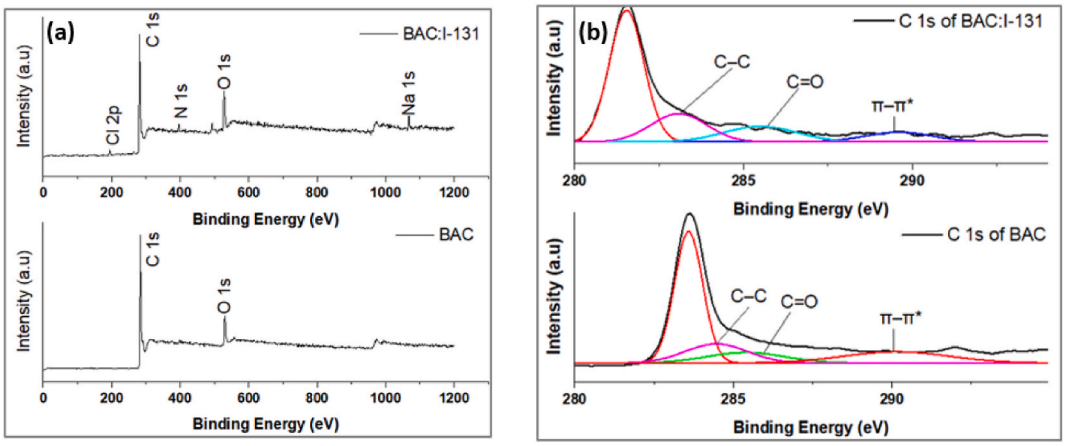

Fig. 7. (a) Survey XPS spectra of BAC and BAC:I-131, where three new photoelectron peaks existed in BAC:I-131; (b) C 1s core-level spectra of BAC and BAC:I-131 was shifted to the right for π–π* transitions at 287 eV (BAC:I-131) and 290 eV (BAC).

3.2. XPS analysis of adsorbents and sediments

The survey spectrum of GOAg is dominated by three photoelectron peaks that correspond to electrons originating in the 1s orbitals of carbon and oxygen, as well as electrons originating in the 3d orbitals of the Ag atom as shown in Fig. 4 (a). However, the survey spectrum of GOAg:I-131 shows three new photoelectron peaks of Cl 2p, N 1s, and Na 1s as shown in Fig. 4 (b). It can be deduced that GOAg as shown by XPS spectra in Fig. 5 (a) interacts with other elements in I-131 clinical wastewater. The core-level XPS spectra of O 1s show a peak centred at 529.65 eV as shown in Fig. 5 (b), and no new peak was observed after adsorption. This indicates that there is no electron sharing between oxygen atoms and atoms in I-131 wastewater during adsorption. However, the O 1s peak decreased to 529.15 eV, which may be due to ion exchange between oxygen functional groups and I-131 clinical wastewater [19]. In addition, the core-level XPS spectra for C 1s is shown in Fig. 6 (a) for GOAg before and after adsorption. There are three conjunct peaks that can be deconvoluted into different components with binding energies of 284.45 eV due to C = C and 285.35 eV due to C – C or C – H [13]. By comparing the two spectra, it can be observed that the peak intensity of C = C and C – C slightly shifted to the right after the adsorption of I-131 clinical wastewater. Meanwhile, the Ag 3d XPS core-level spectra of GOAg is shown in Fig. 6 (b) with peaks at 364.15 eV and 370.05 eV due to Ag 3d3/2 and Ag 3d5/2, respectively. This suggests that Ag on the GO nanosheets exists in metallic form and was successfully loaded onto the GO nanosheets [20].

The survey spectrum of BAC demonstrates two photoelectron peaks of C 1s and O 1s as shown in 7 (a). On the other hand, the survey spectrum of BAC:I-131 shows three new photoelectron peaks of Cl 2p, N 1s, and Na 1s. It can be deduced that BAC interacts with other elements in I-131 clinical wastewater. High-resolution XPS spectra of C 1s excitation revealed a complex envelope indicating distinct carbon species at the surface of BAC. In Fig. 7 (b), the core-level XPS spectra of C 1s of BAC were resolved into four individual component peaks that represent C – C (284.35 eV), C=O (287.00 eV), and shake-up satellite peaks induced by π–π* transitions in

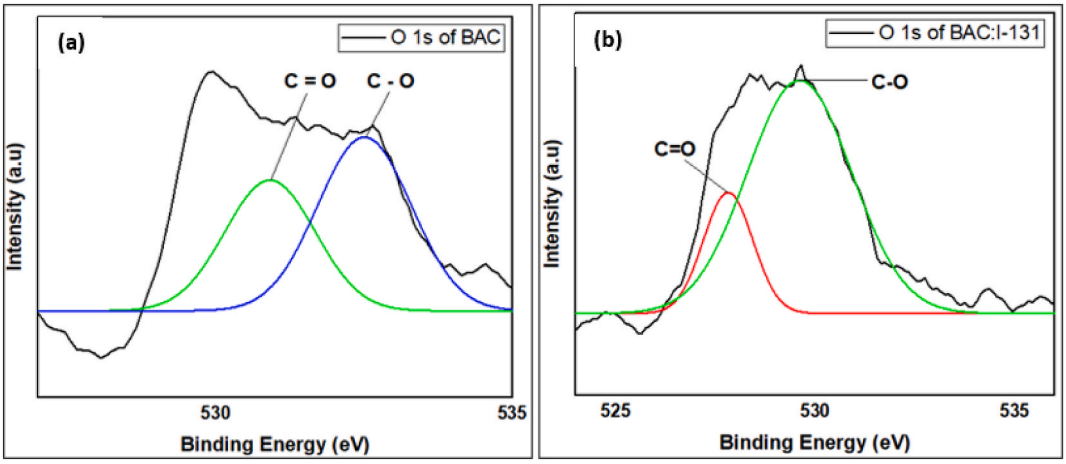

Fig. 8. (a) O 1s core-level spectra of BAC for C = O at 531.0 eV and C – O at 532.65 eV; (b) O 1s core-level spectra of BAC:I-131 for C = O at 528 eV and C – O at 530 eV.

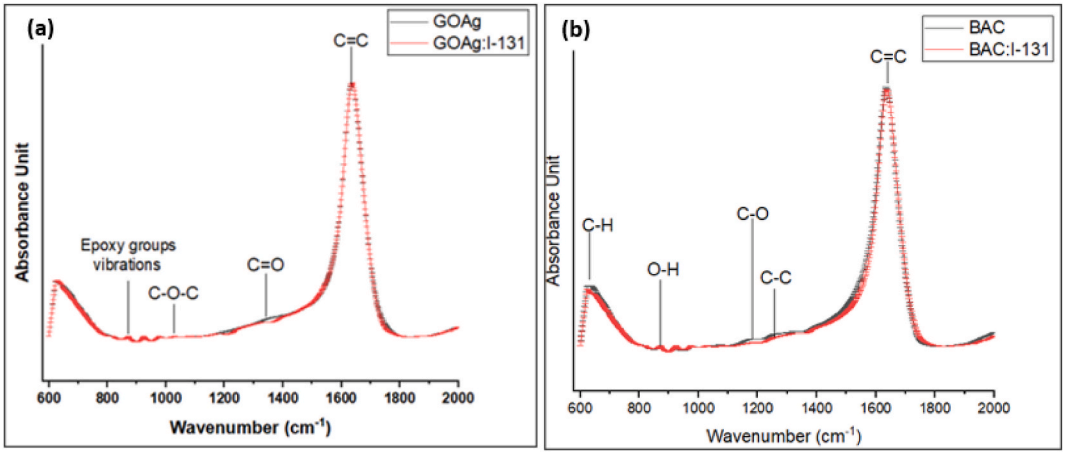

Fig. 9. FTIR spectra before and after adsorption of I-131 wastewater of (a) GOAg and GOAg:I-131; (b) BAC and BAC:I-131.

aromatic rings (290.07 eV) [21,22]. The intensity peaks of C–C and C=O shifted to the right while π–π* transitions shifted to the left after the adsorption of I-131 clinical wastewater. In Fig. 8 (a), the core-level XPS spectra of O 1s show two peaks centred at binding energies of 531.0 eV and 532.65 eV, which can be assigned to C=O and C–O for BAC, respectively [23]. Thus, it can be deduced that the functional groups introduced onto the surface of BAC are mainly hydroxyl, carbonyl, and carboxyl groups. Meanwhile, for BAC:I-131, the C=O and C–O was cantered at 528 eV and 530 eV as shown in Fig. 8 (b).

3.3. FTIR analysis of adsorbents and sediments

Fig. 9 (a) represents the IR spectra of GOAg and GOAg:I-131. The FTIR spectra ranging from 200 cm^{-1} to 2000 cm^{-1} revealed a strong peak for functional groups at 1637.50772 cm^{-1}, which corresponds to carboxylic (C=C) stretching due to the functionalisation process that takes place through the strong bonding of GO functional groups and Ag^{+} ions [24]. The peaks at 1340.48041 cm^{-1} and 1031.88060 cm^{-1} can be ascribed to carbonyl groups (C=O) and vibration of epoxy groups (C–O–C), respectively [25,26]. At peaks between 630.70085 cm^{-1} and 975.94689 cm^{-1}, the presence of the peak at 871.79445 cm^{-1} is due to the stretching vibration of epoxy groups. After the adsorption of I-131 clinical wastewater, the peaks observed in the FTIR spectra of the GOAg:I-131 sediment can be seen in relation to GOAg, although each peak shifted slightly. This can be related to the intercalation of I-131 clinical wastewater within GOAg nanosheets.

Chemical bond availability and appearance changes on the surface of synthesised BAC as adsorbent under KOH activation and BAC:I-131 are shown in Fig. 9 (b). The spectra show a number of absorption peaks, which indicate the potential functional groups present on the BAC surface that may be responsible for the removal of I-131 from the aqueous solution. The highest peak at 1635.57897 cm^{-1} corresponds to the presence of the stretching vibrations of skeletal C=C in aromatic compounds [27]. The second peak at 1257.54421

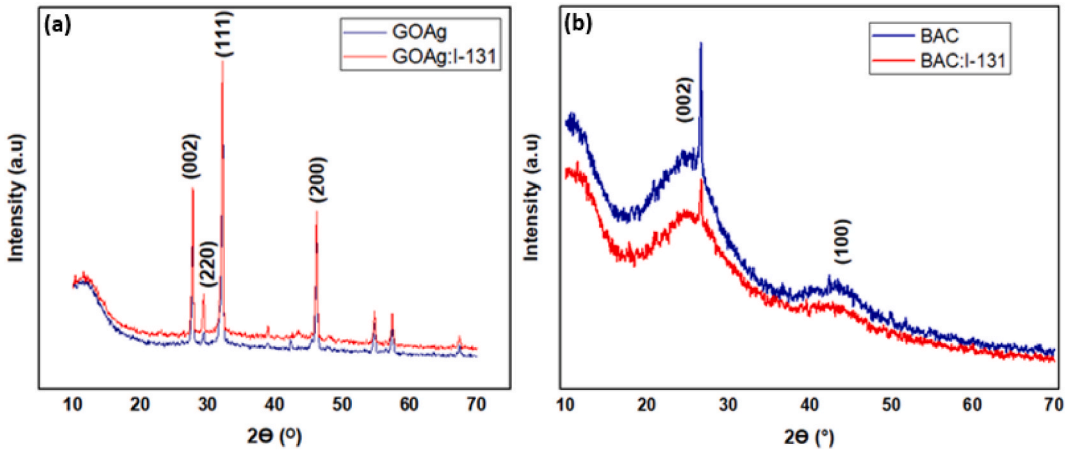

Fig. 10. XRD patterns of (a) GOAg and GOAg:I-131 shows the crystal structures on some plane at 2θ. GOAg:I-131 shows high crystallinity compared to GOAg after adsorption interactions; (b) BAC and BAC:I-131 shows amorphous structures, where the crystallinity was decreased after adsorption interaction (BAC:I-131).

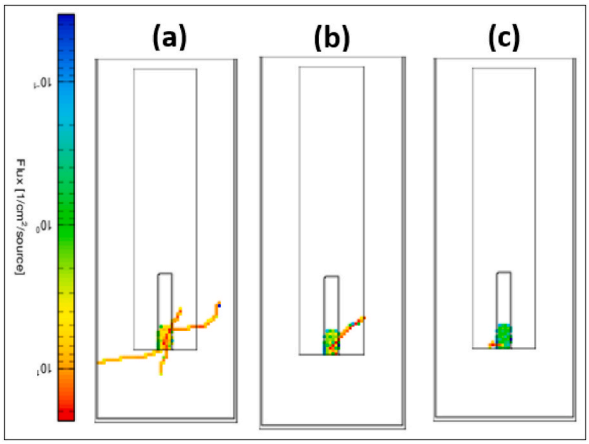

Fig. 11. Side view of β^- particle fluence of GOAg:I-131 sediment at (a) 1.0 mg/mL, (b) 3.0 mg/mL, and (c) 5.0 mg/mL in the dose calibrator.

cm^{-1} is attributed to C–C stretching. These peaks may significantly decrease, most likely due to polysaccharide loss during pyrolysis [7]. Meanwhile, the third peak observed at 1188.10925 cm^{-1} can be assigned to C–O stretching, such as alcohols, ethers, acids, and esters. Other weak peaks were also observed, ranging from 634.55835 cm^{-1} to 871.79445 cm^{-1}, which are associated with C–H and O–H group's out-of-plane bending mode [17]. Compared with BAC, most of the wavenumber peaks in the FTIR spectra of BAC:I-131 sediment shifted slightly towards the lower wavenumber, which may be due to the diffusion of I-131 clinical wastewater within BAC.

3.4. XRD analysis of adsorbents and sediments

Fig. 10 (a) presents the XRD pattern of synthesised GOAg before and after the adsorption of I-131 clinical wastewater. The XRD pattern of GOAg exhibits peaks at 2θ = 27.82°, 29.39°, 32.24°, and 46.22° with d-spacings of 3.20 Å, 3.04 Å, 2.78 Å, and 1.96 Å, respectively. These peaks slightly shifted to the previously reported literature but are still in the accepted range. The intense diffraction peak at 2θ = 27.85° is attributed to the (002) diffraction plane [28]. The diffraction peaks at 2θ = 29.40° and 46.22° can be assigned to (220) and (200) crystallographic planes, respectively, which were indexed based on the Ag FCC structure [29,30]. The peak at 2θ = 32.24° corresponds to the (111) plane of Ag_2O [31]. The crystalline nature of Ag was demonstrated on the XRD pattern of GOAg. The XRD pattern of GOAg:I-131 exhibits almost the same peaks present in GOAg, but there is a minor shift in the peak intensity towards lower 2θ values. This can be deduced from the intercalation of I-131 clinical wastewater within GOAg nanosheets. In addition, the crystallinity index (CrI) of GOAg increased from 37.43 % to 40.66 % after the adsorption of I-131 clinical wastewater.

Fig. 10 (b) shows the XRD pattern of the prepared BAC before and after the adsorption of I-131 clinical wastewater. The BAC has broad peaks centred at 2θ = 26.56° and weak peaks centred at 2θ = 43.58° with d-spacings of 3.35 Å and 2.08 Å, respectively. These two peaks correspond to the hexagonal graphite structure of small crystallites [32]. The peak centred at 2θ = 26.56° can be assigned to

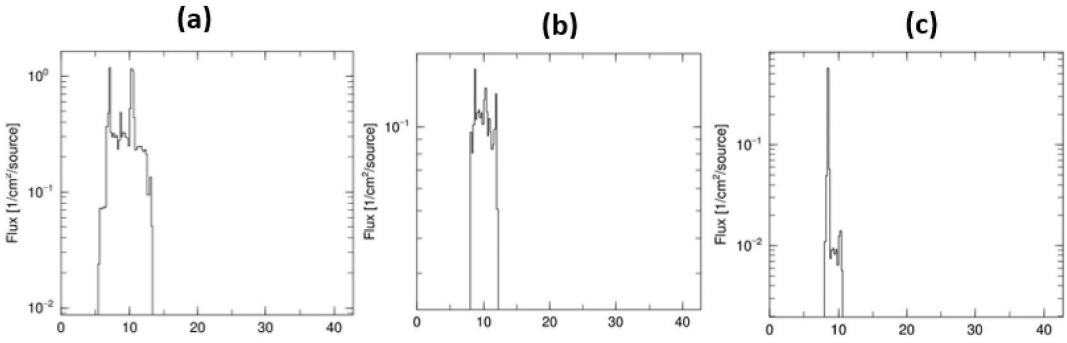

Fig. 12. Energy distribution of β^- particles of GOAg:I-131 sediment at (a) 1.0 mg/mL, (b) 3.0 mg/mL, and (c) 5.0 mg/mL in the dose calibrator.

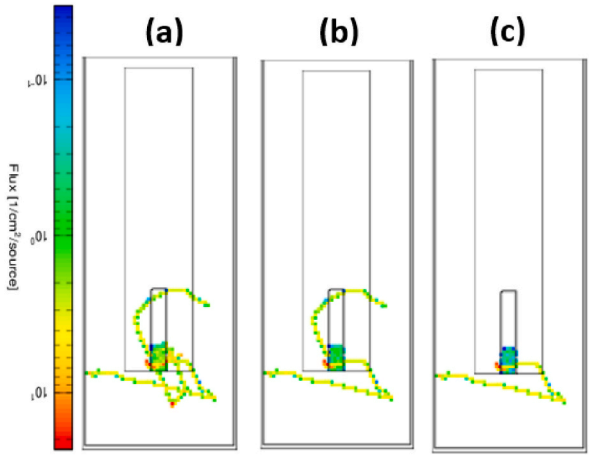

Fig. 13. Side view of β^- particle fluence of BAC:I-131 sediment at (a) 1.0 mg/mL, (b) 3.0 mg/mL, and (c) 5.0 mg/mL in the dose calibrator.

the (002) plane and demonstrates aromatic carbon ring stacking along the c-axis. Meanwhile, the peak centred at $2\theta = 42.41°$ is due to diffraction along the (100) plane. The XRD pattern of BAC mainly consists of amorphous phases, which are in accordance with previously reported literature [33–35]. Moreover, it also has a sharp peak, affirming the formation of certain crystalline graphite structures [36]. The XRD pattern of BAC:I-131 has the same peaks present in BAC, but there is a small shift in the peak intensity towards lower 2θ values. This may be explained by the intercalation of I-131 clinical wastewater within BAC. The crystallinity of BAC decreased from 68.37 % to 58.69 % after adsorption of I-131 clinical wastewater.

3.5. PHITS simulation of β^- particles during adsorption

The fluence of β^- particles is a result of the decay of beta-particle-emitting radionuclides in I-131 wastewater. Based on Fig. 11 (a), the sediment at 1.0 mg/mL shows more fluence of β^- particles than GOAg:I-131 sediment at 3.0 (Fig. 11 (b)) and 5.0 mg/mL (Fig. 11 (c)). This condition is confirmed with energy distribution comparison of β^- particles as shown in Fig. 12(a and b and c). However, the β^- particle fluence became less significant as the concentration of GOAg increased. This indicates that a high concentration of GOAg is more efficient in reducing the radioactivity of I-131 clinical wastewater as active interactions occur at the initial stage of high radioactivity due to the energetic ion interaction between iodine and GOAg at the molecular level. In addition, GOAg is composed of a variety of surface moieties, giving GOAg the ability to easily coagulate with anions in I-131 radionuclide wastewater and to form strong surface complexes via chemisorption during agglomeration.

Fig. 13 shows the simulation on the side view of β^- particle fluence in the dose calibrator of BAC:I-131 sediment with different concentrations. The β^- particle fluence became less significant as the concentration of BAC increased, indicating that a high concentration of BAC is more efficient in the adsorption of I-131 clinical wastewater. This is due to the presence of various functional groups on the BAC surface that actively trap the radionuclide molecules at high concentrations. In contrast, the β^- particle fluence of the sediment at 1.0 mg/mL as shown in Fig. 13 (a) is more significant compared to the BAC:I-131 sediment at 3.0 and 5.0 mg/mL, as shown in Fig. 13 (b) and 13 (c), respectively. This can be deduced that the functional groups and elemental compositions of BAC are able to reduce the radioactivity of I-131 in clinical wastewater by accelerating decay. This is proved by comparing the energy distribution of β^- particles detection using dose calibrator for BAC:I-131 sediments at 1.0 mg/mL, 3.0 mg/mL and 5.0 mg/mL as shown in Fig. 14 (a) and 14 (b) and 14 (c), respectively.

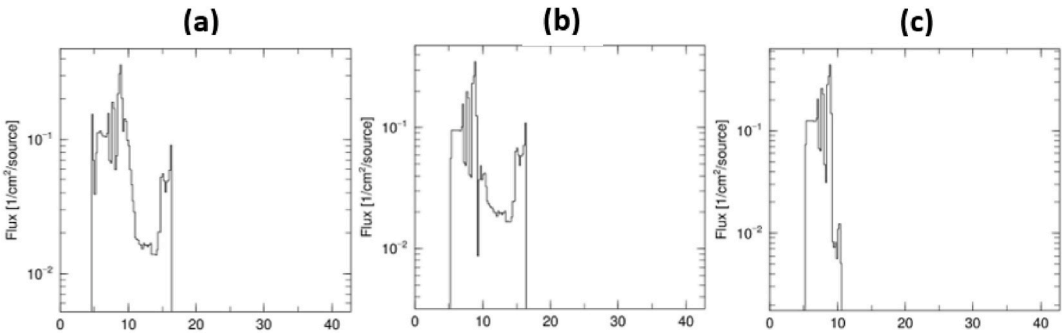

Fig. 14. Energy distribution of β^- particles of BAC:I-131 sediment at (a) 1.0 mg/mL, (b) 3.0 mg/mL, and (c) 5.0 mg/mL in the dose calibrator.

4. Conclusions

In this study, GOAg and BAC primarily demonstrated their capability to isolate I-131 clinical wastewater. The active interaction between I-131 clinical wastewater and oxygen-containing groups within carbon-based adsorbents is clearly shown by the shifted peaks observed in the XPS and FTIR spectra. The crystallinity index for GOAg increased but decreased for BAC after adsorption of I-131 clinical wastewater due to natural structures of synthetic and natural carbon-based materials. Simulation of β^- particles using PHITS shows that the elemental composition of adsorbent at any concentration can reduce the radioactivity of I-131 in clinical wastewater. The finding shows GOAg has high potential as alternative antibacterial radionuclide adsorbent for future clinical radioactive wastewater management in nuclear medicine.

Data availability

Data will be made available on request.

CRediT authorship contribution statement

Rosidah Sunaiwi: Writing – review & editing. **Ruchi Gaur:** Formal analysis, Data curation. **Mohammad Khairul Azhar Abdul Razab:** Writing – review & editing, Supervision. **Fara Hana Hadzuan:** Writing – review & editing. **Norazlina Mat Nawi:** Writing – review & editing. **Mohd Zahri Abdul Aziz:** Writing – review & editing. **An'amt Mohamed Noor:** Writing – review & editing, Methodology. **Nur Atiqah Syahirah Shari:** Validation, Methodology. **Zulhisyam Abdul Kari:** Writing – review & editing, Supervision, Funding acquisition. **Ajay Guru:** Writing – review & editing. **Parashuram Kallem:** Writing – review & editing, Funding acquisition.

Declaration of competing interest

The authors declare that they have no known competing financial interests or personal relationships that could have appeared to influence the work reported in this paper.

Acknowledgement

This work was supported by Universiti Sains Malaysia, Bridging with Project No: R501-LR-RND003-0000000998-0000. We would like to express our appreciation to Mr. Nik Fakurudin Nik Ali and Miss Wan Norhasikin Wan Marizam of the School of Health Sciences, Universiti Sains Malaysia, for their help in obtaining the FESEM micrographs. Our appreciation also goes to the Department of Nuclear Medicine, Radiotherapy, & Oncology, Hospital Universiti Sains Malaysia for their facilities in conducting the research project. Authors also acknowledge financial support from Abu Dhabi University's Office of Research and Sponsored Programs.

References

[1] M.K.A.A. Razab, N.M. Nawi, R. Sunaiwi, A.M. Noor, M.Z.A. Aziz, F.H.M. Hadzuan, F. Ibrahim, A.T. Khaizul, N.H. Abdullah, Efficiency of marketable decontamination agent and graphene oxide on ^{99m}Tc and ^{131}I spillages in nuclear medicine department, Nucl. Technol. Radiat. Protect. 37 (2) (2022) 159–166, https://doi.org/10.2298/NTRP2202159R.

[2] IAEA, Treatment of biomedical radioactive waste, in: Management of Radioactive Waste from the Use of Radionuclides in Medicine, IAEA, Vienna, 2000, pp. 33–50.

[3] N.M. Nawi, N.S. Ahmad, R. Abdullah, W.M.N.W. Zainon, M.K.A.A. Razab, Correlation of external dose rate with whole body clearance estimation in radioiodine therapy for rhTSH and THW patients, Journal of Radiation Research and Applied Sciences 13 (1) (2020) 240–245, https://doi.org/10.1080/16878507.2020.1727675.

[4] A.Y. Romanchuk, A.S. Slesarev, S.N. Kalmykov, D.V. Kosynkinz, J.M. Tour, Graphene oxide for effective radionuclide removal, Phys. Chem. Chem. Phys. 15 (2012) 2321–2327, https://doi.org/10.1039/C2CP44593J.

[5] M.K.A.A. Razab, M.S. Mansor, A.M. Noor, N.F.F.A. Latif, S.M. Rozi, K.N. Jaafar, F. Jamaludin, Characterization of GO:I-131 for radioactive clinical waste water management in nuclear medicine, Mater. Sci. Forum 1010 MSF (2020) 561–566, https://doi.org/10.4028/www.scientific.net/MSF.1010.561.
[6] M.K.A.A. Razab, M.S. Mansor, A.M. Noor, S.M. Rozi, N.F.F.A. Latif, K.N. Jaafar, F. Jamaludin, Preliminary study of the potential graphene oxide as radioactive clinical wastewater adsorbability in nuclear medicine, IOP Conf. Ser. Earth Environ. Sci. 596 (2020), https://doi.org/10.1088/1755-1315/596/1/012037.
[7] Y.A. Waji, Bamboo-based Activated Carbon for Removal of Lead from Aqueous Solution, Addis Ababa Science and Technology University, Ethiopia, 2018. Unpublished Master Thesis.
[8] T. Afrin, T. Tsuzuki, R.K. Kanwar, X. Wang, The origin of the antibacterial property of bamboo, J. Textil. Inst. 103 (8) (2012) 844–849, https://doi.org/10.1080/00405000.2011.614742.
[9] D. Giannakoudakis, T. Bandosz, 1 - graphite oxide nanocomposites for air stream desulfurization, Composite Nanoadsorbents (2019) 1–24, https://doi.org/10.1016/B978-0-12-814132-8.00001-0.
[10] Z. Zhu, M. Su, L. Ma, L. Ma, D. Liu, Z. Wang, Preparation of graphene oxide–silver nanoparticle nanohybrids with highly antibacterial capability, Talanta 117 (2013) 449–455, https://doi.org/10.1016/j.talanta.2013.09.017.
[11] A.M. Noor, N.F.A. Yusoff, H.N. Ming, Z.A. Kari, M.K.A.A. Razab, M.H.A. Bakar, L.S. Wei, N.H. Abdullah, Facile preparation of graphene oxide silver aerogel for antibacterial, Journal of Tropical Resources and Sustainable Science 6 (2018) 41–44, https://doi.org/10.47253/jtrss.v6i1.726.
[12] C. Zhaoa, L. Ge, X. Li, M. Zuo, C. Xua, S. Chen, Q. Li, Y. Wang, C. Xu, Effects of the carbonization temperature and intermediate cooling mode on the properties of coal-based activated carbon, Energy 273 (2023) 1–9, https://doi.org/10.1016/j.energy.2023.127177.
[13] E. Akgun, E. Ozgence, E. Gundogdu, Therapeutic applications of radiopharmaceuticals: an overview, Fabad J. Pharm. Sci. 46 (1) (2021) 93–104.
[14] Q. Bao, D. Zhang, P. Qi, Synthesis and characterization of silver nanoparticle and graphene oxide nanosheet composites as a bactericidal agent for water disinfection, J. Colloid Interface Sci. 360 (2) (2011) 463–470, https://doi.org/10.1016/j.jcis.2011.05.009.
[15] P. Poolprasert, T. Chorchong, Preparation of activated carbon from cassava root for cadmium removal in aqueous solution sample, Journal of Renewable Energy and Smart Grid Technology 15 (2) (2020) 26–38.
[16] B.C. Kim, Y.H. Kim, T. Yamamoto, Adsorption characteristics of bamboo activated carbon, Kor. J. Chem. Eng. 25 (5) (2008) 1140–1144, https://doi.org/10.1007/s11814-008-0187-y.
[17] N.M. Zawawi, F. Hamzah, S.F.A. Manaf, M. Sarif, A. Idris, Characterization of activated carbon using chemical activation via microwave ultrasonic system, Malaysian Journal of Analytical Science 21 (1) (2017) 159–165, https://doi.org/10.17576/mjas-2017-2101-18.
[18] N.H. Abdullah, M. Mohamed, N.A.M. Shohaimi, A.M. Lazim, A.Z.A. Halim, N.M. Shukri, M.K.A.A. Razab, Enhancing the decolorization of methylene blue using a low-cost super-absorbent aided by response surface methodology, Molecules 26 (15) (2021) 4430, https://doi.org/10.3390/molecules26154430.
[19] M. Song, Y. Wei, S. Cai, L. Yu, Z. Zhong, B. Jin, Study on adsorption properties and mechanism of PB2+ with different carbon based adsorbents, Sci. Total Environ. 618 (2018) 1416–1422, https://doi.org/10.1016/j.scitotenv.2017.09.268.
[20] X. Chen, X. Wang, D. Fang, A review on c1s XPS-spectra for some kinds of carbon materials, Fullerenes, Nanotub. Carbon Nanostruct. 28 (12) (2020) 1048–1058, https://doi.org/10.1080/1536383x.2020.1794851.
[21] Z. Tan, J. Qiu, H. Zeng, H. Liu, J. Xiang, Removal of elemental mercury by bamboo charcoal impregnated with H_2O_2, Fuel 90 (4) (2011) 1471–1475, https://doi.org/10.1016/j.fuel.2010.12.004.
[22] X. Ma, H. Yang, L. Yu, Y. Chen, Y. Li, Preparation, surface and pore structure of high surface area activated carbon fibers from bamboo by steam activation, Materials 7 (6) (2014) 4431–4441, https://doi.org/10.3390/ma7064431.
[23] Q.-S. Liu, T. Zheng, N. Li, P. Wang, G. Abulikemu, Modification of bamboo-based activated carbon using microwave radiation and its effects on the adsorption of methylene blue, Appl. Surf. Sci. 256 (10) (2010) 3309–3315, https://doi.org/10.1016/j.apsusc.2009.12.025.
[24] P. Lozovskis, V. Jankauskaitė, A. Guobienė, V. Kareivienė, A. Vitkauskienė, Effect of graphene oxide and silver nanoparticles hybrid composite on p. Aeruginosa strains with acquired resistance genes, Int. J. Nanomed. 15 (2020) 5147–5163, https://doi.org/10.2147/IJN.S235748.
[25] S. Kumari, P. Sharma, S. Yadav, J. Kumar, A. Vij, P. Rawat, S. Kumar, C. Sinha, J. Bhattacharya, C.M. Srivastava, S. Majumder, A novel synthesis of the graphene oxide-silver (go-AG) nanocomposite for unique physiochemical applications, ACS Omega 5 (10) (2020) 5041–5047, https://doi.org/10.1021/acsomega.9b03976.
[26] D. Prodan, M. Moldovan, G. Furtos, C. Saroși, M. Filip, I. Perhaița, R. Carpa, M. Popa, S. Cuc, S. Varvara, D. Popa, Synthesis and characterization of some graphene oxide powders used as additives in hydraulic mortars, Appl. Sci. 11 (23) (2021) 11330, https://doi.org/10.3390/app112311330.
[27] J. Zhang, Z. Zhong, D. Shen, J. Zhao, H. Zhang, M. Yang, W. Li, Preparation of bamboo-based activated carbon and its application in direct carbon fuel cells, Energy & Fuels 25 (5) (2011) 2187–2193, https://doi.org/10.1021/ef200161c.
[28] S.N. Alam, N. Sharma, L. Kumar, Synthesis of graphene oxide (GO) by Modified Hummers method and its thermal reduction to obtain reduced graphene oxide (rGO), Graphene 6 (1) (2017) 1–18, https://doi.org/10.4236/graphene.2017.61001.
[29] M. Vivek, P.S. Kumar, S. Steffi, S. Sudha, Biogenic silver nanoparticles by gelidiella acerosa extract and their antifungal effects, Avicenna J. Med. Biotechnol. (AJMB) 3 (3) (2011) 143–148.
[30] M.R. Das, R.K. Sarma, S.C. Borah, R. Kumari, R. Saikia, A.B. Deshmukh, M.V. Shelke, P. Sengupta, S. Szunerits, R. Boukherroub, The synthesis of citrate-modified silver nanoparticles in an aqueous suspension of graphene oxide nanosheets and their antibacterial activity, Colloids Surf. B Biointerfaces 105 (2013) 128–136, https://doi.org/10.1016/j.colsurfb.2012.12.033.
[31] Y.-L. Kuo, H.-W. Chen, Y. Ku, Analysis of silver particles incorporated on TiO_2 coatings for the photodecomposition of O-Cresol, Thin Solid Films 515 (7–8) (2007) 3461–3468, https://doi.org/10.1016/j.tsf.2006.10.085.
[32] B. Lu, L. Hu, H. Yin, X. Mao, W. Xiao, D. Wang, Preparation and application of capacitive carbon from bamboo shells by one step molten carbonates carbonization, Int. J. Hydrogen Energy 41 (41) (2016) 18713–18720, https://doi.org/10.1016/j.ijhydene.2016.05.083.
[33] A. Ip, J. Barford, G. McKay, Production and comparison of high surface area bamboo derived active carbons, Bioresour. Technol. 99 (18) (2008) 8909–8916, https://doi.org/10.1016/j.biortech.2008.04.076.
[34] M.A. Mohamed, W.N.W. Salleh, J. Jaafar, M.S. Rosmi, Z.A. Mohd Hir, M.A. Mutalib, A.F. Ismail, M. Tanemura, Carbon as amorphous shell and interstitial dopant in mesoporous rutile Tio2: bio-template assisted sol-gel synthesis and photocatalytic activity, Appl. Surf. Sci. 393 (2017) 46–59, https://doi.org/10.1016/j.apsusc.2016.09.145.
[35] M.-J. Jung, E. Jeong, S. Kim, S.I. Lee, J.S. Yoo, Y.S. Lee, Fluorination effect of activated carbon electrodes on the electrochemical performance of electric double layer capacitors, J. Fluor. Chem. 132 (12) (2011) 1127–1133, https://doi.org/10.1016/j.jfluchem.2011.06.046.
[36] L. Jena, D. Soren, P.K. Deheri, P. Pattojoshi, Preparation, characterization and optical properties evaluations of bamboo charcoal, Current Research in Green and Sustainable Chemistry 4 (2021) 100077, https://doi.org/10.1016/j.crgsc.2021.100077.